10) Morooka, S., K. Uchida and Y. Kato: *J. Chem. Eng. Japan*, **15**, 29 (1982).
11) Muroyama, K., K. Hashimoto, T. Kawabata and M. Shiota: *Kagaku Kogaku Ronbunshu*, **4**, 622 (1978).
12) Østergaard, K. and M. L. Michelsen: *Can. J. Chem. Eng.*, **47**, 107 (1969).
13) Vail, Yu. K., N. Kh. Manakov and V. V. Manshilin: *Int. Chem. Eng.*, **8**, 516 (1968).

AN EXPERIMENTAL AND THEORETICAL STUDY ON COMBINED EFFECT OF FREE AND FORCED CONVECTIONS ON MASS TRANSFER BETWEEN TWO LIQUIDS

MITSUNORI HOZAWA, TAKAO TSUKADA, TOHRU KONDO, NOBUYUKI IMAISHI AND KATSUHIKO FUJINAWA
Chemical Research Institute of Non-Aqueous Solutions, Tohoku University, Sendai 980

Key Words: Mass Transfer, Liquid-Liquid System, Free Convection, Forced Convection, Extraction, Mass Transfer Coefficient, Numerical Simulation, Finite Element Method

The combined effect of free and forced convections on mass transfer between two liquids was studied experimentally and theoretically.

In the experiments, steady-state dissolution rates into flowing water of an aniline or furfural drop which was sandwiched between a capillary and a rod and had a nearly cylindrical surface were measured, and the continuous-phase mass transfer coefficients were obtained. During an experimental run, the amount of the drop phase dissolved into water was supplied continuously through the capillary and the drop volume was kept constant.

It was observed that the *Sh* values depend on the flow direction of water in the range of $5 < Re < 100$ and that in the case of upward flow, *Sh* takes the minimum at some *Re* number.

Numerical simulations of the phenomena were tried, using the finite element method, and the experimental results are explained qualitatively.

Introduction

Knowledge of the mechanism of mass and momentum transfer between two liquids is the basis for design of liquid-liquid extraction apparatus.

However, as the hydrodynamics around a two-liquid interface is complicated, especially in the low Reynolds number region where both free and forced convections are important, the exact mechanism of mass transfer has been unknown both experimentally and theoretically.

Pearson and Dickson[6] and one of the authors[3,4] studied continuous-phase mass transfer from an organic drop on a nozzle tip to flowing water and found that free convection either reinforces or retards the mass transfer rates. But possibly their experimental conditions of flow around the drop were not steady-state in the strict sense, because they measured the mass transfer rates from the volume change of the drop and it seemed to take considerable time for the flow around the drop to reach steady state.

The first aim of this work is to confirm their experimental findings with an improved experimental technique that provides steady-state measurement.

The second aim is to analyze theoretically the combined effect of free and forced convections in liquid-liquid systems.

The analysis presents two difficulties: (1) The properties of the two liquids affect the flow, and (2) the interface is mobile and is subject to deformation by gravitational force and interfacial tension.

The authors[9] applied the finite element method to the analysis of motion and deformation of moving bubbles and drops. The same numerical technique was used in this work, though there is an additional problem of coupling of flow and concentration fields.

1. Experimental

Figure 1 shows the experimental apparatus, which consists of an annular column of 8 mm i.d., 24.6 mm o.d. and 120 mm height.

An organic drop which is partly soluble in water, aniline or furfural was sandwiched between a glass or

Received December 4, 1984. Correspondence concerning this article should be addressed to M. Hozawa. T. Kondo is now with Chiyoda Chem. Eng. & Construction Co., Ltd.

Table 1. Physical properties of the liquids at 298 K

	ρ [kg/m^3]	ρ_i [kg/m^3]	μ [Pa·s]	μ_i [Pa·s]	D_C*) [m^2/s]	C* [mol/m^3]	σ**) [mN/m]
Aniline	0.102×10^4	0.999×10^3	0.381×10^{-2}	0.960×10^{-3}	0.108×10^{-8}	0.393×10^3	4.80
Furfural	0.115×10^4	0.101×10^4	0.151×10^{-2}	0.107×10^{-2}	0.112×10^{-8}	0.781×10^3	5.13
Water	0.997×10^3	—	0.890×10^{-3}	—	—	—	—

*) Calculated values by Sitaraman's equation.[8]
**) Values at 293 K.

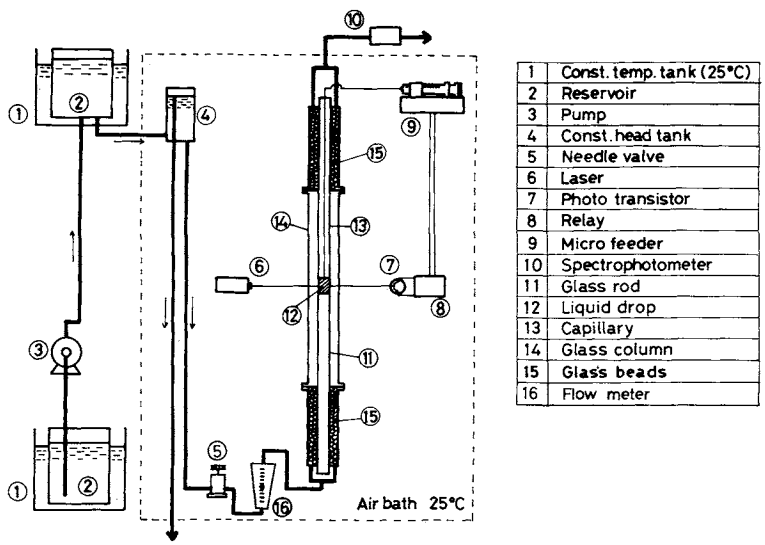

Fig. 1. Experimental apparatus.

Teflon capillary*[1] (8 mm o.d. and 1 mm i.d.) on the upper side and a glass rod (8 mm o.d.) on the lower side. The organic phase was first saturated with water. Distilled water was made to flow through the annular section both upward and downward and the rates of dissolution of the organic liquid were investigated.

The amount of organic phase dissolved into water was supplied through the capillary ⑬ from the microfeeder ⑨, using a control system with the He-Ne laser ⑥ and a phototransistor ⑦ that can detect the position of the interface. Therefore, the drop volume was kept constant during each experimental run. Thus measurements at steady state were made possible.

Mass transfer rates were evaluated by measuring the concentration of the aqueous solution at the column outlet with a spectrophotometer.

The continuous-phase mass transfer coefficient k_C was calculated by Eq. (1).

$$k_C = C'_{out}Q/AC^* \tag{1}$$

The interfacial area A was obtained from a numerical integration of a photograph of the drop profile. All experiments were carried out at 298 K. **Table 1** shows the physical properties of the liquids used.

*[1] Taking account of the wettability of the nozzle surface by the organic liquid, glass and Teflon capillaries were used respectively for aniline and furfural.

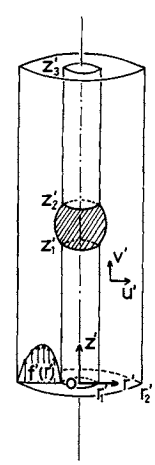

Fig. 2. Cylindrical coordinates.

2. Theory

Figure 2 shows the cylindrical coordinates used for the numerical analysis.

The steady-state equations of motion for the continuous and the dispersed phases are given by Eqs. (2) and (3).

$$-\nabla'\cdot\rho_C\boldsymbol{v}'_C\boldsymbol{v}'_C-\nabla' p'_C-\nabla'\cdot\boldsymbol{\tau}'_C+\rho_C\boldsymbol{g}=0 \tag{2}$$

$$-\nabla'\cdot\rho_D\boldsymbol{v}'_D\boldsymbol{v}'_D-\nabla' p'_D-\nabla'\cdot\boldsymbol{\tau}'_D+\rho_D\boldsymbol{g}=0 \qquad (3)$$

where suffixes C and D mean continuous and dispersed phases respectively.

The continuity equations are described as follows.

$$\nabla'\cdot\boldsymbol{v}'_C=0 \qquad (4)$$

$$\nabla'\cdot\boldsymbol{v}'_D=0 \qquad (5)$$

The diffusion equation in the continuous phase is expressed by Eq. (6).

$$\boldsymbol{v}'_C\cdot\nabla' C'=D_C\nabla'^2 C' \qquad (6)$$

Physical properties are assumed to be constant and are evaluated at $C'=0$, the only exception being for the density dependence on concentration to allow for the effect of buoyancy.

$$\rho_C=\rho_{C,0}+C'(\partial\rho_C/\partial C') \qquad (7)$$

Equation (7) is applied only to the gravitational term in Eq. (2).

The boundary conditions are expressed as follows.

At inflow plane ($z'=0$):

$$\boldsymbol{n}\cdot\boldsymbol{v}'_C=f'(r') \qquad (8a)$$

$$\boldsymbol{t}\cdot\boldsymbol{v}'_C=0 \qquad (8b)$$

$$C'=0 \qquad (8c)$$

At outflow plane ($z'=z'_3$):

$$\boldsymbol{n}\cdot\boldsymbol{\tau}'_C=0 \qquad (8d)$$

$$\partial C'/\partial z'=0 \qquad (8e)$$

At inside and outside walls ($r'=r'_1$, $r'=r'_2$):

$$\boldsymbol{n}\cdot\boldsymbol{v}'_C=\boldsymbol{n}\cdot\boldsymbol{v}'_D=0 \qquad (8f)$$

$$\boldsymbol{t}\cdot\boldsymbol{v}'_C=\boldsymbol{t}\cdot\boldsymbol{v}'_D=0 \qquad (8g)$$

$$\partial C'/\partial r'=0 \qquad (8h)$$

At liquid-liquid interface:

$$\boldsymbol{n}\cdot\boldsymbol{v}'_C=\boldsymbol{n}\cdot\boldsymbol{v}'_D=0 \qquad (8i)$$

$$\boldsymbol{t}\cdot\boldsymbol{v}'_C=\boldsymbol{t}\cdot\boldsymbol{v}'_D \qquad (8j)$$

$$\boldsymbol{\tau}'_C:\boldsymbol{nt}=\boldsymbol{\tau}'_D:\boldsymbol{nt} \qquad (8k)$$

$$p'_D+\boldsymbol{\tau}'_D:\boldsymbol{nn}=p'_C+\boldsymbol{\tau}'_C:\boldsymbol{nn}+2H'\sigma \qquad (8l)$$

$$C'=C^* \qquad (8m)$$

where $\boldsymbol{n}$ is the outward-pointing normal and $\boldsymbol{t}$ is the tangential unit vector at the boundary.

The shape of the drop was determined by Eq. (8l). As the experiments were carried out in the low Re number region, the dynamic terms ($\boldsymbol{\tau}'_D:\boldsymbol{nn}$ and $\boldsymbol{\tau}'_C:\boldsymbol{nn}$) in Eq. (8l) were neglected.

To solve the above problem, the Galerkin finite element method (F.E.M.)[5,7,9] was used.

The finite element formulations in a dimensionless expression are described in **Appendix 1**.

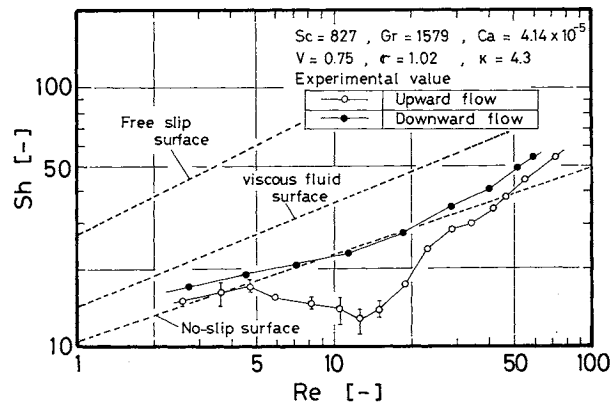

Fig. 3. *Sh* vs. *Re* in aniline–water system.

3. Results and Discussion

3.1 Experimental results

Figure 3 shows the experimental relations between the Sherwood number and the Reynolds number for the aniline-water system, where the drop height is 6 mm.

The three dotted lines in Fig. 3 indicate the theoretical predictions for $Gr=0$, which were obtained by a simple numerical technique (see **Appendix 2**).

As the density of aqueous solution of aniline and furfural increases with increasing concentration, free convection occurs. The direction of the free convection is opposite to that of the forced convection when water flows upward (upward flow), while it is identical in the case of downward flow.

From Fig. 3, the following points are revealed: (1) In the high Re region, $Re>50$, experimental Sh values in either upward or downward flow approach those given by the theory of viscous fluid surface, where forced convection is dominant. (2) In the intermediate Re region, $5\leqq Re\leqq 50$, Sh values depend on the flow direction of the continuous phase. In the case of upward flow, Sh value takes the minimum at $Re\fallingdotseq 10$, differently from the case of downward flow. (3) In the low Re region, $Re<5$, the experimental Sh values of both cases agree again and approach a constant value which depends on Gr number, where free convection is dominant.

In the case of downward flow, it is expected that the experimental Sh values would be larger than the theoretical values for a viscous fluid surface. But apparently the experimental Sh values rather agree with the theory of no-slip surface even in the high Re number region. This fact suggests that circulation inside the drop was hindered more or less by a trace amount of impurities, although the liquids were carefully handled so as not to be contaminated.

In **Fig. 4**, the data for the aniline–water system ($Gr=1579$) are compared to those of the furfural–

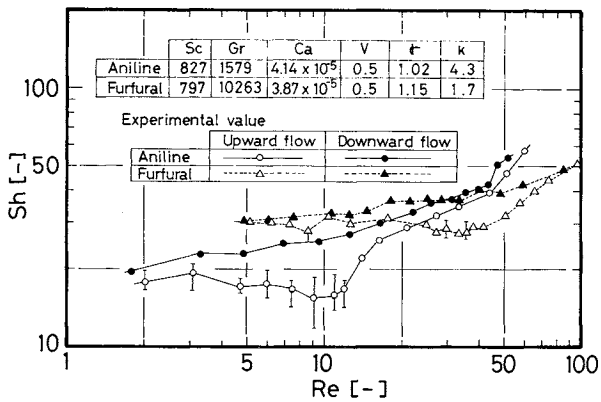

Fig. 4. Effect of *Gr* on *Sh*.

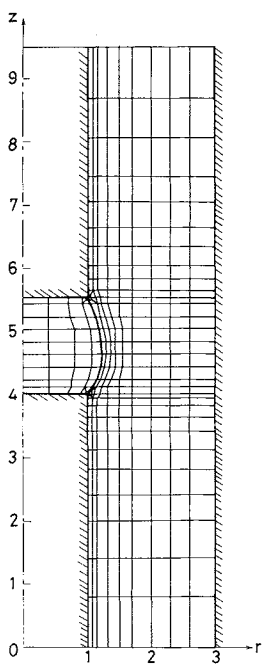

Fig. 5. Discretization of calculation domain for finite element method.

water system ($Gr = 10263$). The drop heights are 4 mm in both systems. It is apparent that the *Re* value at which *Sh* takes the minimum increases with increasing *Gr* value.

In conclusion, the experimental results can be explained by the interaction between free and forced convections, and they agree with the findings of Peason and Dickson[6] and one of the authors.[3,4]

3.2 Theoretical results

To the authors' regret, the exact simulation of the experimental systems was very difficult, because the *Sc* number and the *Gr* number are too large for us to obtain reasonable numerical results; that is, the required memory and computation time exceeded the capacity of the computer. Therefore, calculations for hypothetical conditions of $Sc = 1$, 10 and $Gr = 100$–500 were carried out. The other parameters were kept identical to the experimental conditions.

The accuracy of the calculations was checked by comparing the *Sh* value obtained from integration of the concentration gradient at the two-liquid interface with that from the average concentration of the continuous phase at the outlet.

For the numerical analyses, the calculation domain was discretized as shown in **Fig. 5**. The grid has 318 elements, 1045 nodes and 3511 freedoms.

Figures 6 and **7** show the calculated velocity vectors and concentration distribution for $Re = 3.5$ and $Re = 10$ respectively. The parameters are based on the properties of the aniline-water system except *Sc* and *Gr* in Figs. 6–9.

From Fig. 6, it is apparent that a descending flow due to free convection is prevailing near the interface and a large circulation arises in the continuous phase. The concentration boundary layer is thick for $Re = 3.5$, as shown in Fig. 6(b).

In the case of $Re = 10$, as shown in Fig. 7, circulation in the continuous phase vanishes, since forced convection becomes dominant. Apparently, free convection retards the mass transfer in the case of upward flow.

Figure 8 shows the effect of interfacial shape on the flow pattern. Figure 8(a) shows the case for a relatively flat interface and Fig. 8(b) is for a convex interface. Apparently, from Fig. 8, the circulation inside the drop is larger for the convex surface than for the flat one.

Figure 9 shows the calculated *Sh*–*Re* relations for various choices of *Gr* and *Sc* where the drop shape is the same as in Figs. 6 and 7. Apparently, dependencies of *Sh* on *Re* and *Gr* similar to the experimental results in Figs. 3 and 4 are observed when $Sc = 10$. At $Sc = 1$, the minimum point in *Sh*–*Re* relation in the case of upward flow disappears.

Figure 10 shows the calculated velocity vectors and concentration distribution in the case of upward flow for $Re = 10$. The calculations are based on the properties of the furfural–water system, in which the shape of the surface is relatively complicated.

It is seen that the finite element method is suitable for simulations of mass and momentum transfer through a two-liquid surface which is mobile and is subject to deformation. It must be noted, however, that the exact simulation of the coupling problem of mass and momentum is difficult for such systems with high *Sc* and *Gr* as in this experimental case.

Conclusion

The combined effect of free and forced convections on mass transfer between two liquids were investigated experimentally and theoretically, and the following conclusions are obtained.

(1) When the effect of free convection exists, the

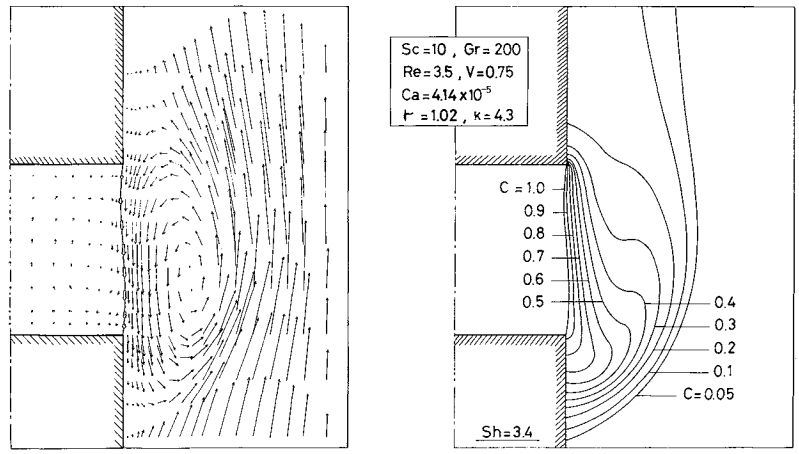

Fig. 6. Velocity vectors and concentration distribution for upward flow.

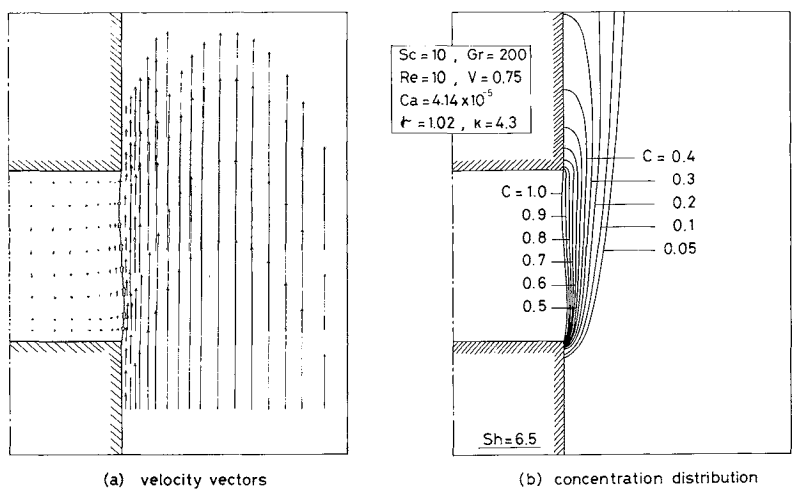

Fig. 7. Velocity vectors and concentration distribution for upward flow.

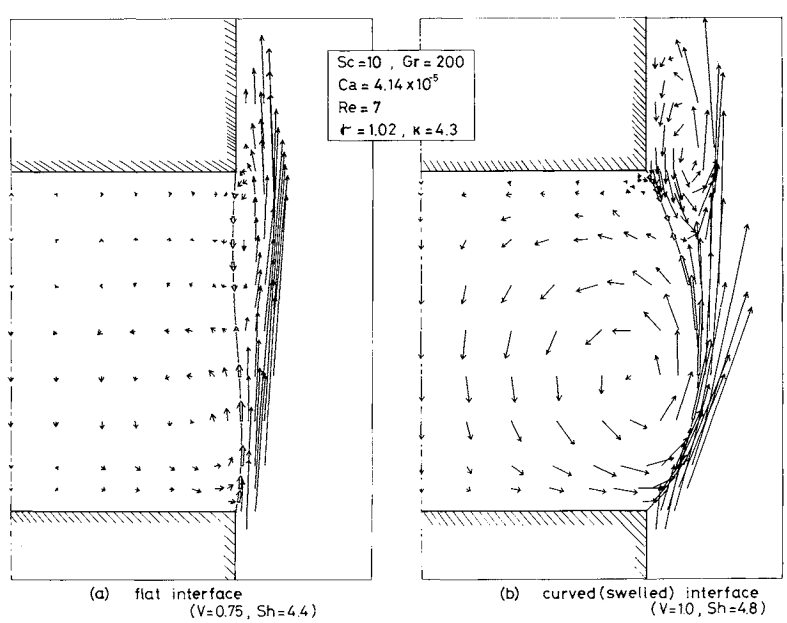

Fig. 8. Effect of interfacial shapes on velocity vectors around the interface for upward flow.

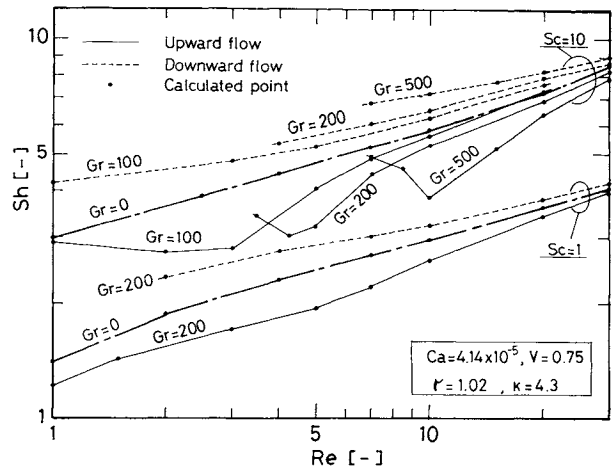

Fig. 9. Calculated relations between *Sh* and *Re*.

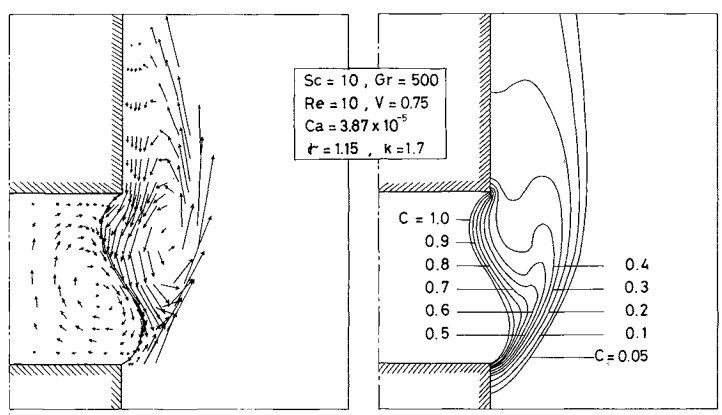

Fig. 10. Velocity vectors and concentration distribution for upward flow.

flow patterns and concentration profiles are influenced by the direction of forced convection. In the case of upward flow, *Sh* takes the minimum value at some *Re*, which increases with increasing *Gr*.

(2) The finite element method is useful for the numerical analysis of transport phenomena through a two-liquid surface, although it was difficult to simulate exactly the experiments with high *Sc* and high *Gr*.

(3) From the numerical analyses, the geometry of the interface apparently affects the circulation inside the drop.

Acknowledgment

This research was supported in part by a Grant-in-Aid for Scientific Research (No. 59550640) of the Ministry of Education, Science and Culture, Japan. The authors are grateful to Mr. M. Kojima (Nissinbo Industries Inc.) for his cooperation in the experimental work. The numerical calculations were carried out by use of the ACOS 1000 of the Computer Center of Tohoku Univ.

Appendix 1

In each finite element consisting of an eight-node quadrilateral, the nondimensional velocity $\boldsymbol{v}$, pressure p, and concentration C are approximated as follows.

$$\boldsymbol{v}(r, z)=\sum \phi^i \boldsymbol{v}_i \tag{A-1}$$

$$p(r, z)=\sum \psi^k p_k \tag{A-2}$$

$$C(r, z)=\sum \phi^i C_i \tag{A-3}$$

where quadratic trial function ϕ^i is used for $\boldsymbol{v}$ and C, and linear trial function ψ^k is used for p.

Substitution of Eqs. (A-1)–(A-3) into the non-dimensional forms of Eqs. (2)–(8) gives the following algebraic equations.

The equations of motion:

$$\int_V (\nabla\phi^i \cdot \boldsymbol{T}_C+\phi^i \boldsymbol{v}_C \cdot \nabla \boldsymbol{v}_C+\phi^i GrC)dV-\int_S \phi^i \boldsymbol{T}_C \cdot \boldsymbol{n}dS=0 \tag{A-4}$$

$$\int_V \{\nabla\phi^i \cdot \boldsymbol{T}_D+(\rho_D/\rho_C)\phi^i \boldsymbol{v}_D \cdot \nabla \boldsymbol{v}_D\}dV-\int_S \phi^i \boldsymbol{T}_D \cdot \boldsymbol{n}dS=0 \tag{A-5}$$

where $\boldsymbol{T}_C=-p_C\boldsymbol{I}+(\nabla \boldsymbol{v}_C+\nabla \boldsymbol{v}_C^T)$, $\boldsymbol{T}_D=-p_D\boldsymbol{I}+(\mu_D/\mu_C)(\nabla \boldsymbol{v}_D+\nabla \boldsymbol{v}_D^T)$ and S means the boundary surface of the domain V.

The continuity equations:

$$\int_V \psi^k(\nabla \cdot \boldsymbol{v}_C)dV=0 \tag{A-6}$$

$$\int_V \psi^k(\nabla \cdot \boldsymbol{v}_D)dV=0 \tag{A-7}$$

The diffusion equation:

$$\int_V \{(1/Sc)\nabla\phi^i \cdot \nabla C+\phi^i \boldsymbol{v}_C \cdot \nabla C\}dV-(1/Sc)\int_S \phi^i \nabla C \cdot \boldsymbol{n}dS=0 \tag{A-8}$$

The dimensionless boundary conditions are expressed as follows.
At inflow plane:

$$\boldsymbol{n}\cdot\boldsymbol{v}_C=f(r) \tag{A-9}$$

$$\boldsymbol{t}\cdot\boldsymbol{v}_C=0 \tag{A-10}$$

$$C=0 \tag{A-11}$$

At outflow plane:

$$\boldsymbol{\tau}_C\cdot\boldsymbol{n}=0 \tag{A-12}$$

$$\partial C/\partial z=0 \tag{A-13}$$

At inside and outside walls:

$$\boldsymbol{n}\cdot\boldsymbol{v}_C=\boldsymbol{n}\cdot\boldsymbol{v}_D=0 \tag{A-14}$$

$$\boldsymbol{t}\cdot\boldsymbol{v}_C=\boldsymbol{t}\cdot\boldsymbol{v}_D=0 \tag{A-15}$$

$$\partial C/\partial r=0 \tag{A-16}$$

At liquid-liquid interface:

$$\boldsymbol{n}\cdot\boldsymbol{v}_C=\boldsymbol{n}\cdot\boldsymbol{v}_D=0 \tag{A-17}$$

$$\boldsymbol{t}\cdot\boldsymbol{v}_C=\boldsymbol{t}\cdot\boldsymbol{v}_D \tag{A-18}$$

$$\boldsymbol{\tau}_C:\boldsymbol{nt}=(\mu_D/\mu_C)\boldsymbol{\tau}_D:\boldsymbol{nt} \tag{A-19}$$

$$Ca\boldsymbol{T}_D:\boldsymbol{nn}+Bo_D(z-z_{0D})-p_{0D}$$
$$=Ca\boldsymbol{T}_C:\boldsymbol{nn}+Bo_Cz-2H \tag{A-20}$$

$$C=1 \tag{A-21}$$

where $f(r)$ is assumed to be expressed by the following laminar flow pattern.

$$f(r)=[2Re/\{1+\eta^2-(1-\eta^2)/\ln(1/\eta)\}]$$
$$\times[\eta^2-\eta^2r^2+\{(1-\eta^2)/\ln(1/\eta)\}\ln r] \tag{A-22}$$

The flow and the concentration field are determined by solving Eqs. (A-4)–(A-8) with the boundary conditions, Eqs. (A-9)–(A-21). For the diffusion equation of Eq. (A-8), the upwind finite element method developed by Heinrich *et al.*[1] was used to preclude spurious oscillation of the convection-diffusion problem. The set of nonlinear coupled algebraic equations, Eqs. (A-4)–(A-8), was solved by an iterative Newton-Raphson scheme. To solve the matrix equations, the frontal method developed by Hood[2] was used.

Appendix 2

When there is no coupling between mass and momentum, Sh can be calculated by use of a simple finite difference scheme under the following assumptions,

1) The shape of the surface is exactly cylindrical.
2) Diffusion in the axial direction is negligible in comparison with that in the radial direction.

The diffusion equation in a dimensionless form is expressed as follows.

$$v(\partial C/\partial z)=(1/Sc)\{\partial(r\partial C/\partial r)/\partial r\cdot r)\} \tag{A-23}$$

The boundary conditions are

$$C=0 \quad \text{at} \quad z=z_1 \tag{A-24}$$

$$C=1 \quad \text{at} \quad r=1 \tag{A-25}$$

$$dC/dr=0 \quad \text{at} \quad r=r_b \tag{A-26}$$

where r_b is the position of the concentration boundary layer outside which C can be set to be 0.

The calculation domain can be restricted in the range of $z_1<z<z_2$, and $1<r<r_b$.

v is independent of C and is expressed as follows.

For no slip surface,

$$v=f(r) \tag{A-27}$$

For free slip surface,

$$v=[2Re/\{1-3\eta^2+4\eta^4\ln(1/\eta)/(1-\eta^2)\}]$$
$$\times\{1-\eta^2r^2+2\eta^2\ln(\eta r)\} \tag{A-28}$$

For viscous fluid surface,

$$v=B[1-\eta^2r^2+(-v_i/B+1-\eta^2)$$
$$\times\ln(\eta r)/\ln(1/\eta)] \tag{A-29}$$

$$B=[Re\ln(1/\eta)/\{-0.5+\eta^2\ln(1/\eta)/(1-\eta^2)\}+v_i]/$$
$$[1-\eta^2+(1-\eta^2)\ln(1/\eta)/$$
$$\{-1+2\eta^2\ln(1/\eta)/(1-\eta^2)\}] \tag{A-30}$$

where v_i is the average velocity of v at the two-liquid interface and was obtained by solving Eqs. (A-4)–(A-7) using the finite element method for the drop with cylindrical shape.

Equation (A-23) was solved numerically, using a finite difference method.

Nomenclature

A	=	area of liquid-liquid interface	[m^2]
B	=	parameter defined by Eq. (A-30)	[—]
Bo	=	Bond number ($=\rho g r_1'^2/\sigma$)	[—]
C'	=	concentration	[mol·m^{-3}]
C^*	=	equilibrium concentration	[mol·m^{-3}]
C'_{out}	=	solute concentration at outlet	[mol·m^{-3}]
C	=	C'/C^*	[—]
Ca	=	Capillary number ($=\rho_C v_C'^2/r_1'\sigma$)	[—]
D_C	=	diffusion coefficient	[m^2·s^{-1}]
f'	=	velocity distribution function	[m·s^{-1}]
f	=	$f'r_1'/v_C$	[—]
Gr	=	Grashof number ($=r_1'^3 g\Delta\rho/\rho_C v_C'^2$)	[—]
g	=	gravitational acceleration	[m·s^{-2}]
H'	=	curvature of interface	[m^{-1}]
H	=	$H'\cdot r_1'$	[—]
$\boldsymbol{I}$	=	unit tensor	[—]
k_C	=	continuous-phase mass transfer coefficient	[m·s^{-1}]
$\boldsymbol{n}$	=	outward-pointing normal at boundary surface	[—]
p'	=	pressure	[Pa]
p_0'	=	pressure at reference position	[Pa]
p_C	=	$(p_C'-\rho_C g z')/\rho_C v_C'^2$	[—]
p_D	=	$(p_D'-p_{0D}'-\rho_D g z')\rho_C v_C'^2$	[—]
Q	=	volume flow rate	[m^3·s^{-1}]
Re	=	Reynolds number ($=r_1'v_0'/v_C$)	[—]
r'	=	radial distance in cylindrical coordinates	[m]
r_1', r_2'	=	inner and outer radius of annular tube	[m]
r	=	r'/r_1'	[—]
r_b	=	position of concentration boundary layer	[—]
Sc	=	Schmidt number ($=v_C/D_C$)	[—]
Sh	=	Sherwood number ($=k_C r_1'/D_C$)	[—]
$\boldsymbol{T}_C$	=	$-p_C\boldsymbol{I}+(\nabla\boldsymbol{v}_C+\nabla\boldsymbol{v}_C^T)$	[—]
$\boldsymbol{T}_D$	=	$-p_D\boldsymbol{I}+(\mu_D/\mu_C)(\nabla\boldsymbol{v}_D+\nabla\boldsymbol{v}_D^T)$	[—]
$\boldsymbol{t}$	=	tangential unit vector at boundary surface	[—]
u'	=	radial component of velocity vector	[m·s^{-1}]
V'	=	drop volume	[m^3]
V	=	$V'/2\pi r_1'^3$	[—]
v'	=	axial component of velocity vector	[m·s^{-1}]
$\boldsymbol{v}'$	=	velocity vector	[m·s^{-1}]
v_0'	=	average velocity of continuous phase	[m·s^{-1}]
$v, \boldsymbol{v}, v_0$	=	$v'r_1'/v_C$, $\boldsymbol{v}'r_1'/v_C$, $v_0'r_1'/v_C$	[—]
z'	=	axial component of cylindrical coordinates	[m]
z	=	z'/r_1'	[—]

γ	$= \rho_D/\rho_C$	[—]
κ	$= \mu_D/\mu_C$	[—]
η	$= r_1'/r_2'$	[—]
ν	= kinematic viscosity	$[m^2 \cdot s^{-1}]$
μ	= viscosity	[Pa·s]
ρ	= density	$[kg \cdot m^{-3}]$
$\Delta\rho$	$= \rho_i - \rho_C$	$[kg \cdot m^{-3}]$
σ	= interfacial tension	$[mN \cdot m^{-1}]$
τ_C'	$= -\mu_C(\nabla' v_C' + \nabla' v_C'^T)$	[Pa]
τ_D'	$= -\mu_D(\nabla' v_D' + \nabla' v_D'^T)$	[Pa]
τ	$= \tau' r_1'/\rho_C v_C^2$	[—]
ϕ^i, ψ^k	= trial function	[—]

〈Subscripts〉

C	= continuous phase
D	= drop phase
i	= value of continuous phase saturated with drop phase
0	= value at $C'=0$

Literature Cited

1) Heinrich, J. C. and O. C. Zienkiewicz: *Int. J. Num. Meth. Eng.*, **11**, 1831 (1977).
2) Hood, P.: *Int. J. Num. Meth. Eng.*, **10**, 379 (1976).
3) Hozawa, M.: Doctoral Dissertation of Tohoku Univ., 1974.
4) Hozawa, M. and T. Tadaki: *J. Chem. Eng. Japan*, **10**, 403 (1977).
5) Orr, F. M. and L. E. Scriven: *J. Fluid Mech.*, **84**, 145 (1978).
6) Pearson, R. S. and P. F. Dickson: *AIChE J.*, **14**, 903 (1968).
7) Silliman, W. J. and L. E. Scriven: *J. Comput. Phys.*, **34**, 287 (1980).
8) Sitaraman, R., S. H. Ibrahim and N. R. Kuloor: *J. Chem. Eng. Data*, **8**, 198 (1963).
9) Tsukada, T., M. Hozawa, N. Imaishi and K. Fujinawa: *J. Chem. Eng. Japan*, **17**, 246 (1984).

(Presented at the Third Pacific Chemical Engineering Congress, at Seoul, May 1983.)

AN EXPERIMENTAL STUDY OF MASS TRANSFER RATE IN THE DISPERSED PHASE FOR SINGLE CHARGED DROPS IN A DIELECTRIC LIQUID UNDER A UNIFORM ELECTRIC FIELD

MANABU YAMAGUCHI, TORU TAKAMATSU, FUMIYA YOSHIDA AND TAKASHI KATAYAMA

Department of Chemical Engineering, Faculty of Engineering Science, Osaka University, Toyonaka 560

Key Words: Charged Drops, Drop Formation, Liquid Extraction, Mass Transfer, Uniform Electric Field

Mass transfer of iodine from single charged drops of aqueous iodine solution into a continuous phase of cyclohexane was measured during the overall process of formation, free fall and coalescence of the drops in a range of uniform electric field strength up to 2.4 kV/cm. The total amount of iodine transferred was separated into that during drop formation and that during the subsequent stages. Each mass transfer mechanism during the formation and the free fall of drops in the electric field was investigated with theoretical and empirical equations in the literature, which were obtained in the absence of an electric field.

The mechanism of mass transfer during the formation of the charged drops in the presence of an electric field and that during free fall of the drops are the same as those obtained in the absence of an electric field. The enhancement of mass transfer obtained in the electric field is due to the increased effective interfacial area per volume of dispersed phase and to the increased moving velocity of the drops caused by applying the electric field.

Introduction

In separation processes dealing with liquid drops, various attempts have been made to enhance their mass transfer efficiencies. Generally, enhancement can be obtained by producing a larger interfacial area for diffusion and a higher degree of turbulence within and around drops for eddy diffusion. The requirement for making turbulence coupled with a larger interfacial area is difficult because these features are incompatible in the sense that small drops do not have high relative velocities, nor do they exhibit marked internal circulation patterns. The application of an electric field as a technique to overcome these problems has been proposed by Thornton and coworkers.[2-4,21,22] This technique has the following advantages. Small charged drops can be produced easily by using an electrostatic force,[2-4,17] and the

Received December 7, 1984. Correspondence concerning this article should be addressed to T. Katayama.